SUPPORTING INFORMATION

Monodisperse Ni_3Fe single-crystalline nanospheres as a highly efficient catalyst for the complete conversion of hydrous hydrazine to hydrogen at room temperature

Dong Ge Tong,[*a] Dong Mei Tang,[a] Wei Chu,[*b] Gui Fang Gu[a] and Ping Wu[a]

[a]*Mineral Resources Chemistry Key Laboratory of Sichuan Higher Education Institutions, College of Materials and Chemistry & Chemical Engineering, Chengdu University of Technology, Chengdu 610059, China. E-mail: tongdongge@163.com; Fax: +86-28-8407 9074*

[b]*College of Chemical Engineering, Sichuan University, Chengdu 610065, China. E-mail: chuwei65@yahoo.com.cn; Fax: +86-28-8540 3397*

Summary: 16 Pages; 2 Tables; 20 Figures;

Table S1 The effect of reaction parameters, including reaction temperature, reaction time and cetylamine/palmitic acid, Ni/Fe precursors, BTM/(Ni+Fe), $Tl(i\text{-}Bu)_3$/(Ni+Fe) molar ratios on the sphere percentage, average diameter, and chemical composition of Ni_3Fe nanospheres

Sample	Reaction temperature/ ºC	Reaction time /min	Cetylamine/ palmitic acid	Ni/Fe precursors	BTM /(Ni+Fe)	$Tl(i\text{-}Bu)_3$ /(Ni+Fe)	Sphere percentage /%	Average Diameter /nm	Ni/Fe atomic ratio
1	220	30	4:1	1:1	1.3	0.1	100.0	16.7	3.00
2	210	30	4:1	1:1	1.3	0.1	100.0	12.5	3.01
3	200	30	4:1	1:1	1.3	0.1	100.0	8.1	3.00
4	190	30	4:1	1:1	1.3	0.1	80.3	7.8	3.16
5	180	30	4:1	1:1	1.3	0.1	67.2	7.4	3.43
6	160	30	4:1	1:1	1.3	0.1	53.6	6.9	3.84
7	200	60	4:1	1:1	1.3	0.1	100.0	10.1	3.02
8	200	30	3:1	1:1	1.3	0.1	78.6	11.8	3.08
9	200	30	2:1	1:1	1.3	0.1	64.2	15.5	3.14
10	200	30	1:1	1:1	1.3	0.1	51.8	22.1	3.22
11	200	30	5:1	1:1	1.3	0.1	93.2	9.6	2.98
12	200	30	4:1	2:1	1.3	0.1	95.7	8.9	3.04
13	200	30	4:1	1:2	1.3	0.1	80.1	7.7	3.17
14	200	30	4:1	1:1	1.2	0.1	84.5	13.1	3.05
15	200	30	4:1	1:1	1.0	0.1	60.3	9.0	3.13
16	200	30	4:1	1:1	2.0	0.1	83.8	7.7	3.18
17	200	30	4:1	1:1	1.3	0.05	97.4	24.3	3.00
18	200	30	4:1	1:1	1.3	0.03	98.7	18.9	3.00
19	200	30	4:1	1:1	1.3	0.02	99.2	13.1	3.00
20	200	30	4:1	1:1	1.3	0.125	100	8.1	3.00

Table S2 Catalytic performance of different catalysts for N_2H_4 decomposition

Samples	Catalyst concentration /mmolL^{-1}	H_2 generation volume /mL	H_2 selectivity /%	Time/min	TOF /min^{-1}	TTON	ATOF/ min^{-1}
Monodispersed Ni_3Fe nanospheres supported on C in this work	8.0	224.0	100.0	27	9.26	15840	8.8
Aggregated Ni_3Fe supported on C in this work	8.0	179.9	80.3	420	0.59	-	-
In situ Rh_4Ni[20]	12.5	89.6	100.0	160	0.25	-	-
In situ $Ni_{0.93}Pt_{0.07}$[21]	15.6	89.6	100.0	190	0.0021	-	-
In situ $Ni_{0.95}Ir_{0.05}$[22]	62.2	89.6	100.0	390	0.26	-	-
NiFe[23]	-	89.6	100.0	190	-	-	-
Ni_3Fe[23]	-	79.7	89.0	225	-	-	-
$NiFe_3$[23]	-	63.6	71.0	240	-	-	-
In situ $Rh_{4.69}Ni$/graphene[24]	9.0	89.6	100.0	49	1.91	-	-
Co-B nanospheres[44]	-	954.2	21.3	23	5.34	-	-
Co-B honeycomb[45]	-	1872.6	41.8	13	12.6	18360	10.2
9.86wt%Fe-B/MWCNTs[46]	-	4345.6	97.0	15.2	67.2	114480	63.6
Ni-Al_2O_3-HT[60]	-	-	93.0	70	0.033	-	-
In-situ $Ni_{0.6}Pd_{0.4}$[61]	-	71.7	80.0	300	-	-	-
$NiPt_{0.057}/Al_2O_3$[62]	-	70.2	98.0	11.5	0.28	-	-

Electronic Supplementary Material (ESI) for Journal of Materials Chemistry A

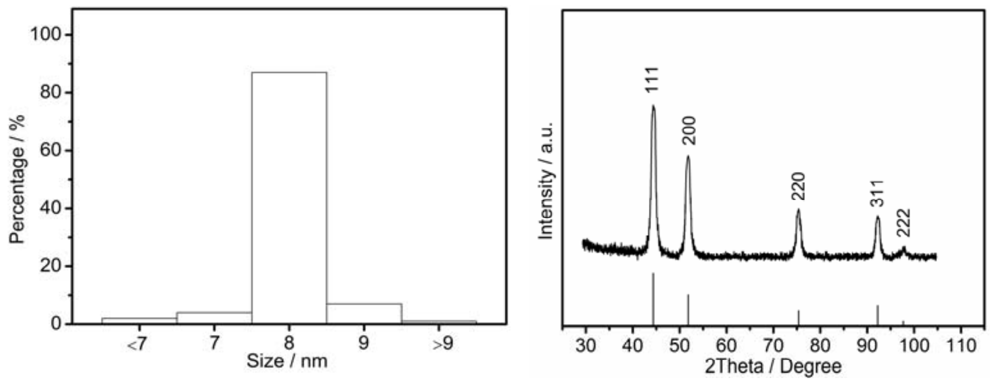

a b

Fig.S1. a) The particle size histogram; b) XRD pattern of the 8.1nm Ni_3Fe nanospheres prepared at the optimized conditions in this work.

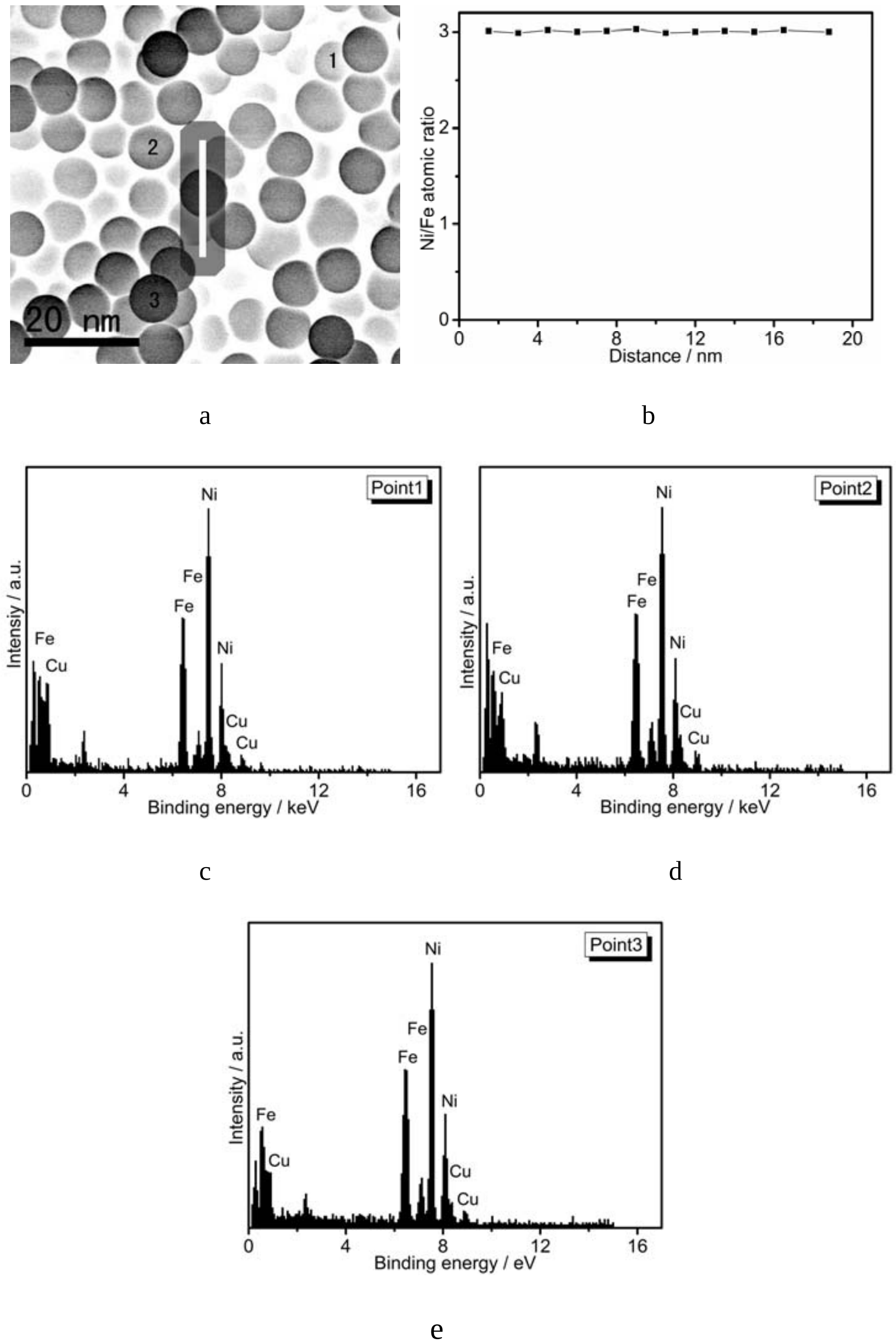

Fig.S2. a)The high-angle annular dark-field scanning transmission electron microscopy (HAADF-STEM); b) Ni/Fe atomic ratio recorded along the cross-sectional compositional line shown in a); c)-e)the Energy-dispersive X-ray spectroscopy (EDS) at points 1-3 in a) of the 8.1nm Ni_3Fe nanospheres prepared at the optimized conditions in this work.

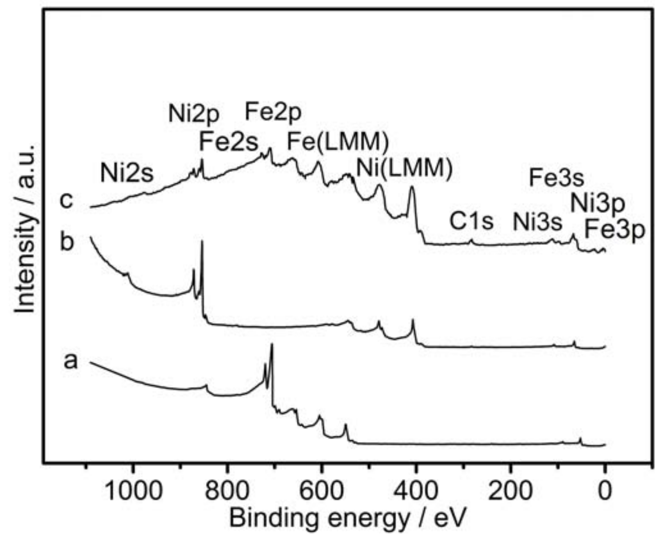

Fig.S3. Overall XPS spectra of (a) Fe, (b) Ni and (c) the 8.1nm Ni_3Fe nanospheres prepared at the optimized conditions in this work.

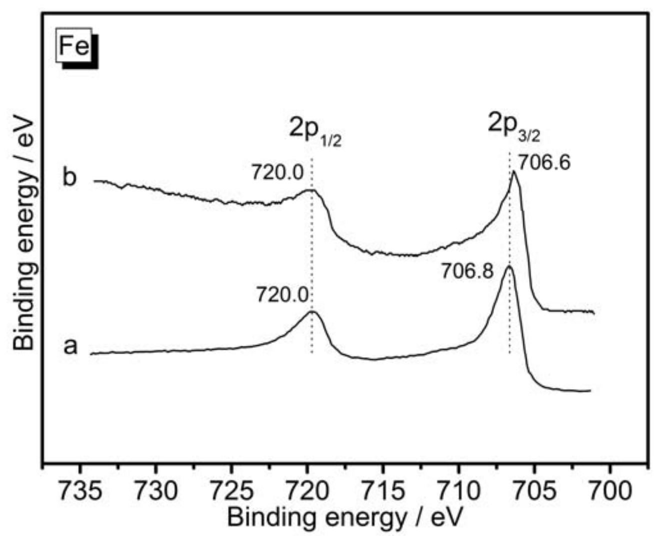

Fig.S4. Fe2p XPS spectra of (a) Fe and (b) the 8.1nm Ni_3Fe nanospheres prepared at the optimized conditions in this work.

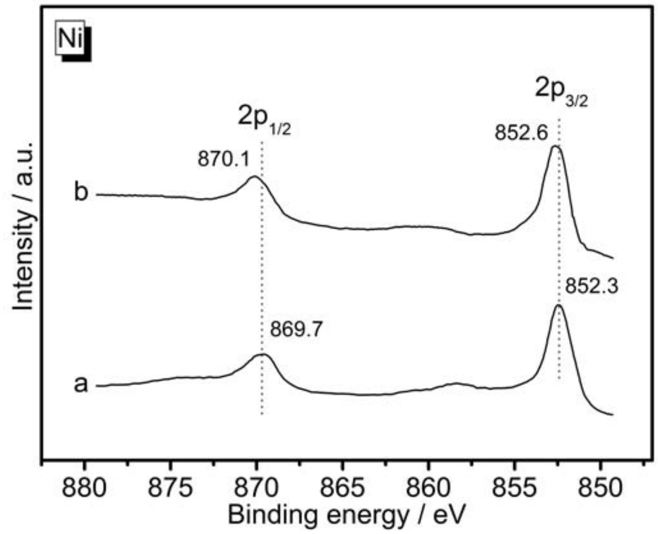

Fig.S5. Ni2p XPS spectra of (a) Ni and (b) the 8.1nm Ni_3Fe nanospheres prepared at the optimized conditions in this work.

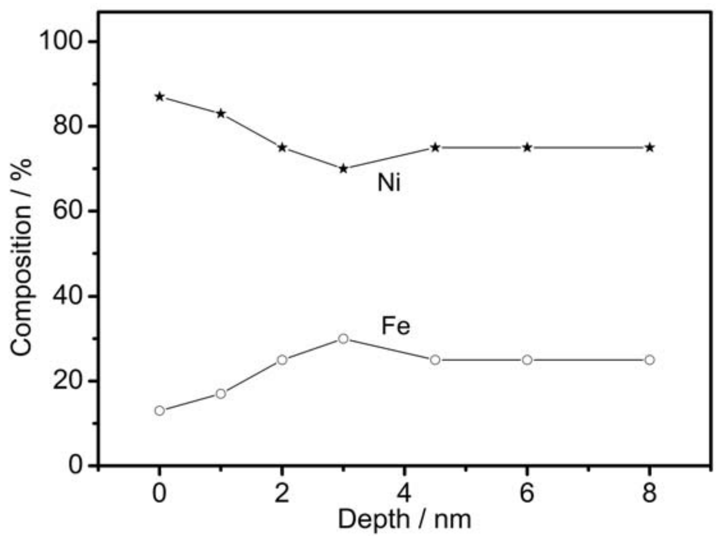

Fig.S6. Depth profile curves obtained using X-ray photoelectron spectroscopy of the 8.1nm Ni_3Fe nanospheres prepared at the optimized conditions in this work.

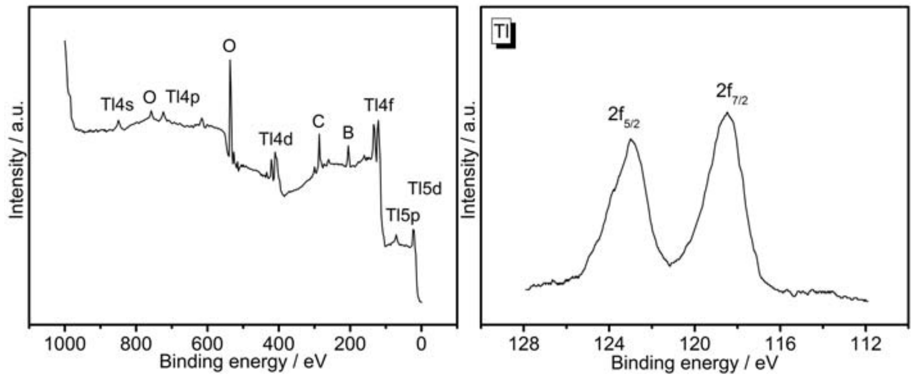

a b

Fig.S7. (a) Overall XPS spectrum and (b) Tl 2f spectrum for the reaction residue after the preparation of Ni_3Fe nanospheres.

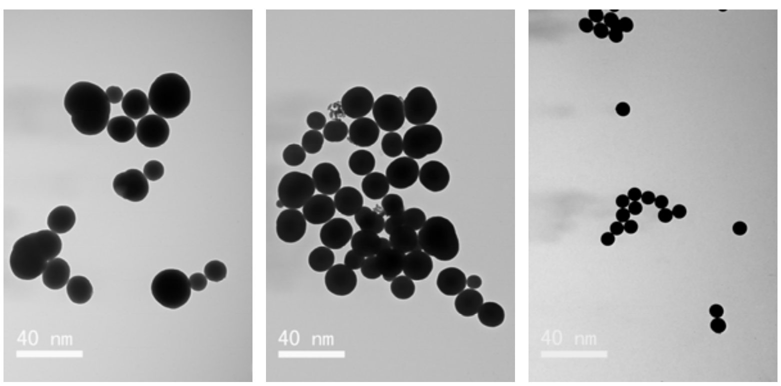

(a) (b) (c)

Fig.S8. TEM images of the Ni_3Fe NPs prepared using a) $Fe(acac)_2$; b) FeC_2O_4 and c) $FeCl_2$ as the iron precursor.

Electronic Supplementary Material (ESI) for Journal of Materials Chemistry A

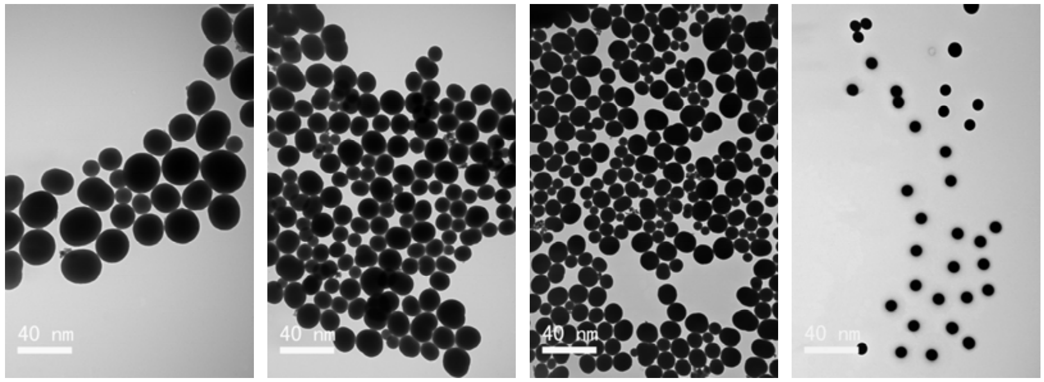

(a) (b) (c) (d)

Fig.S9. TEM images of the Ni_3Fe NPs synthesized by varying the molar ratio of $Tl(Me)_3/(Ni+Fe)$=1:40, 1:30, 1:20 and 1:8, respectively.

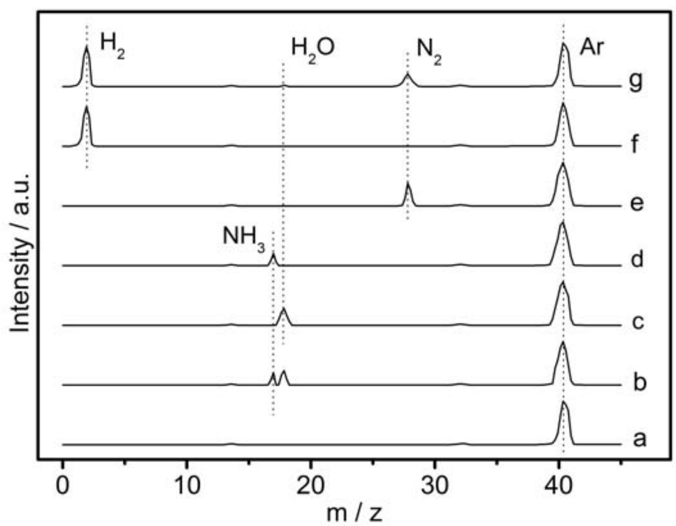

Fig.S10. Mass spectral (MS) profile of (a) carrier Ar; (b) NH_3+H_2O; (c) H_2O; (d) NH_3; (e) N_2; (e) H_2; and (g) the gases released from the complete decomposition of hydrous hydrazine at room temperature over Ni_3Fe/C.

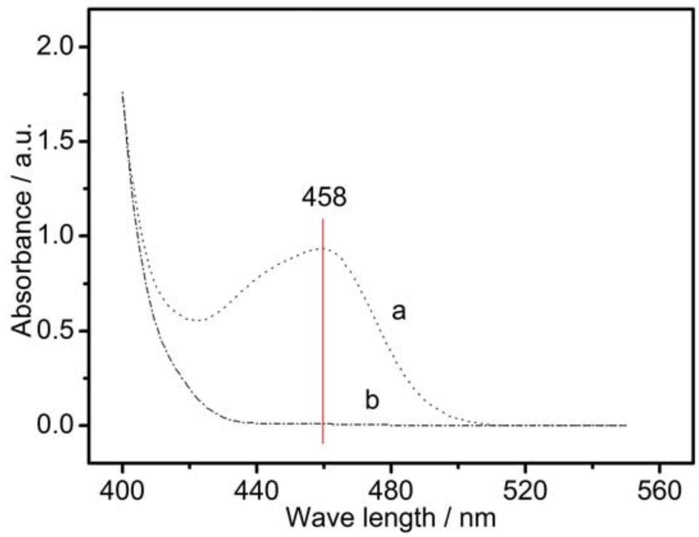

Fig.S11. Typical UV-Vis spectra of hydrous hydrazine (a) before and (b) after the completion of hydrazine decomposition reaction over Ni_3Fe/C.

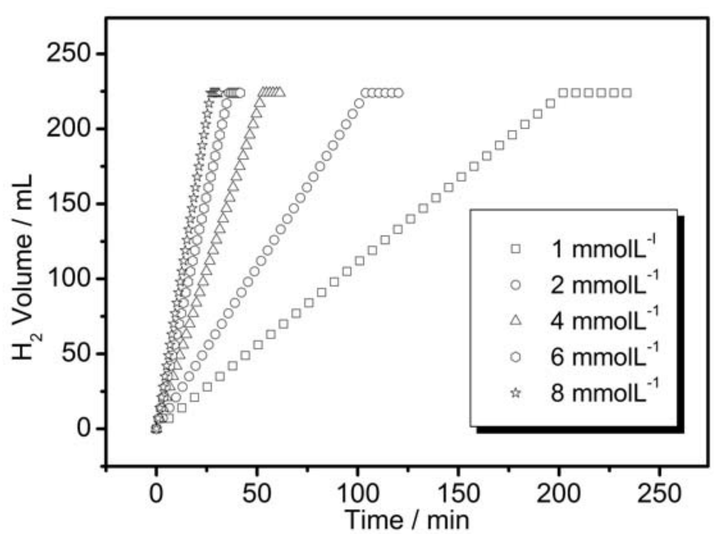

Fig.S12. Plots of volume of hydrogen generated versus time during the hydrazine decomposition over Ni_3Fe/C at different catalyst concentrations ($[N_2H_4]$ = 0.5 molL^{-1}, T = 20±1°C)

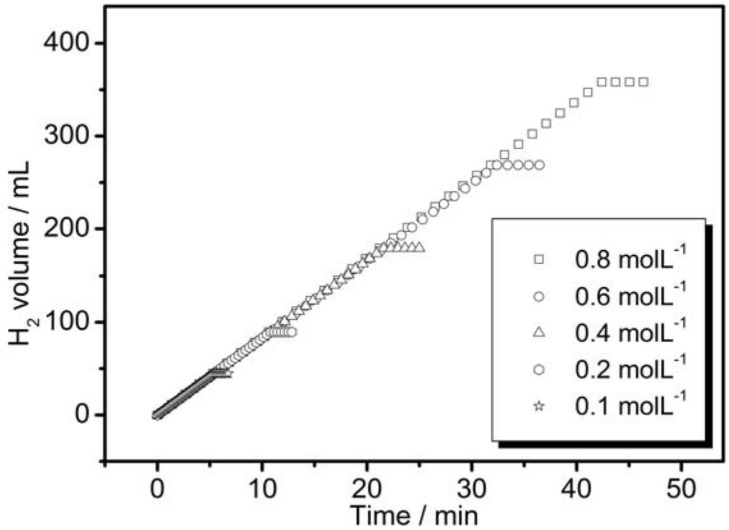

Fig.S13. Plots of volume of hydrogen generated versus time during the hydrazine decomposition over Ni_3Fe/C at different N_2H_4 concentrations ([Ni_3Fe]=8 mmolL^{-1}, T = 20 ± 1 °C).

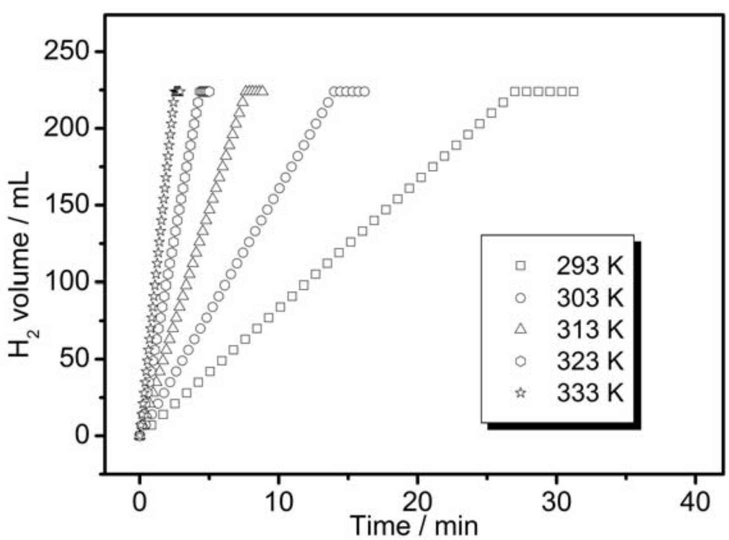

a

Fig.S14. Plots of volume of hydrogen generated versus time during the hydrazine decomposition over Ni_3Fe/C at different temperatures in the range 20-60 °C ([Ni_3Fe] = 8 mmolL^{-1}, [N_2H_4] = 0.5 molL^{-1})

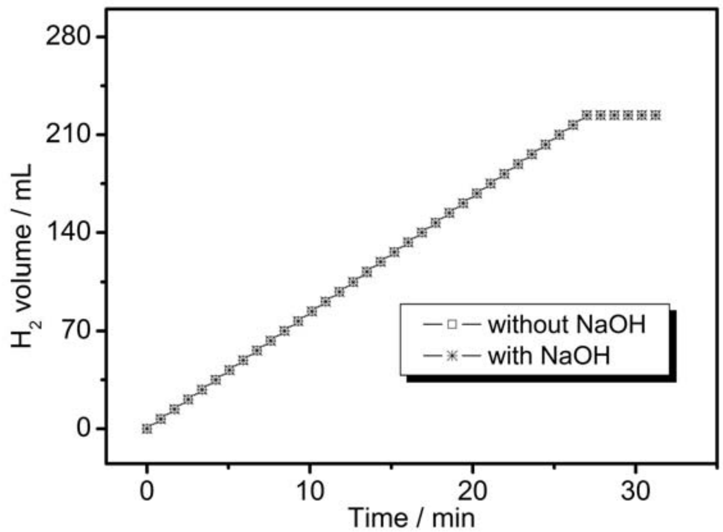

Fig.S15. Plots of volume of hydrogen generated versus time (a) without adding and (b) adding NaOH during the hydrazine decomposition over Ni_3Fe/C.

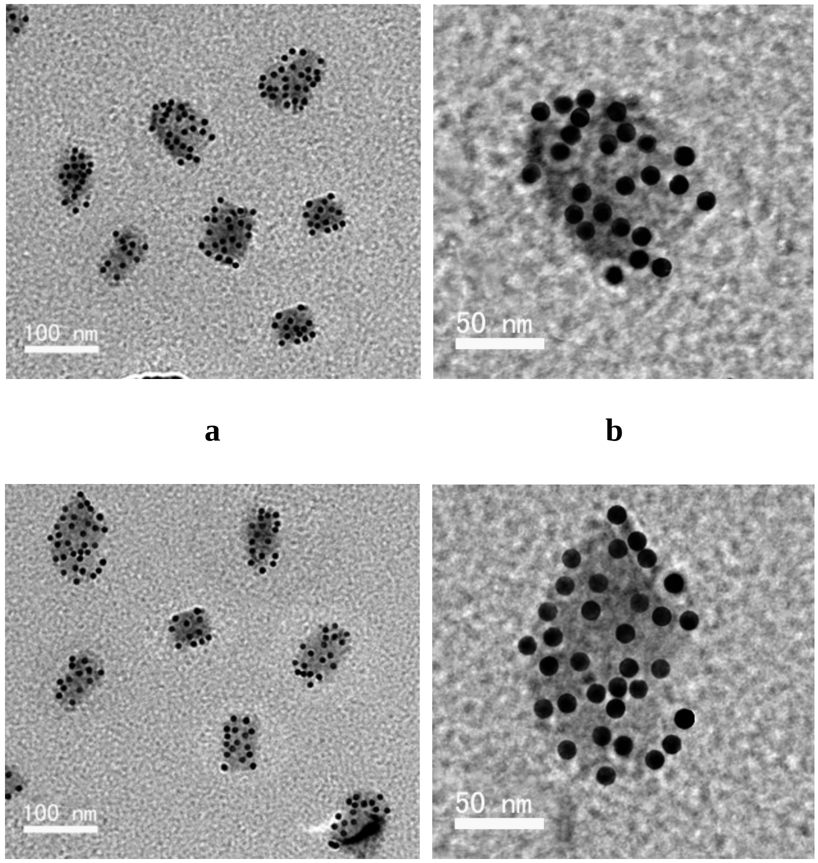

a **b**

c **d**

Fig.S16. (a) TEM image and (b) enlarged TEM image of the deactivated Ni_3Fe/C; (c) TEM image and (d) enlarged TEM image of the deactivated Ni_3Fe/C after reactivation by solution plasma process.

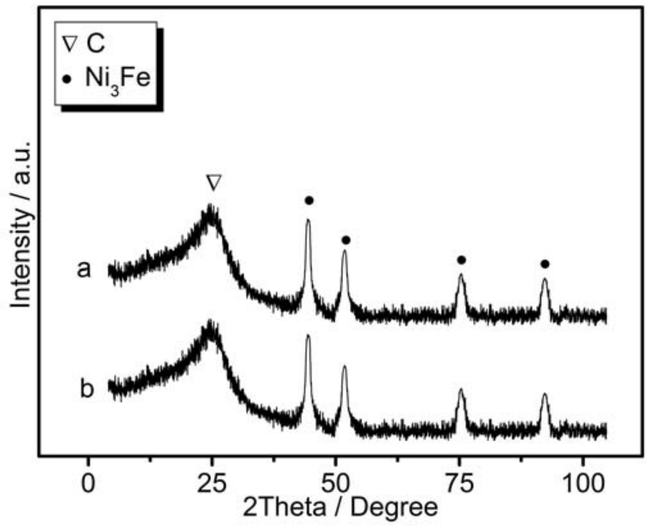

Fig.S17. XRD profiles of the deactivated Ni_3Fe/C (a) before reactivation and (b) after reactivation by solution plasma process.

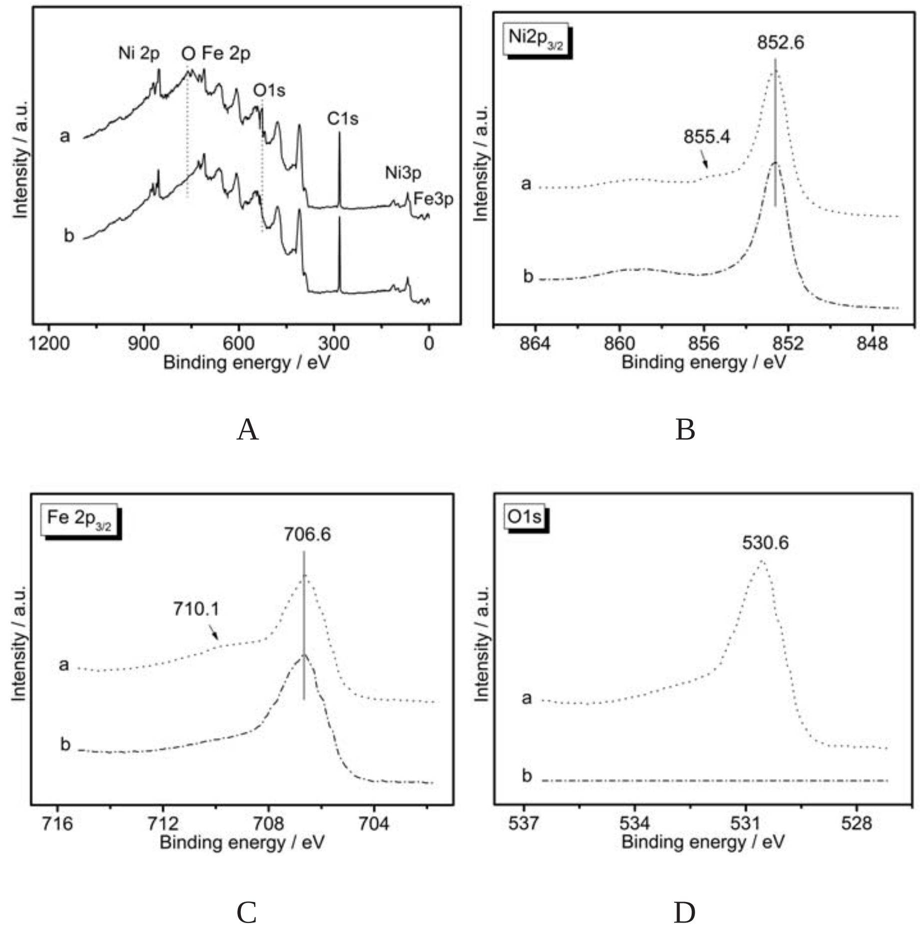

Fig.S18. (A) Overall XPS spectra; (B) $Ni2p_{3/2}$ XPS spectra; (C) $Fe2p_{3/2}$ XPS spectra; and (D) O1s XPS spectra of the deactivated Ni_3Fe/C (a) before reactivation and (b) after reactivation by solution plasma process.

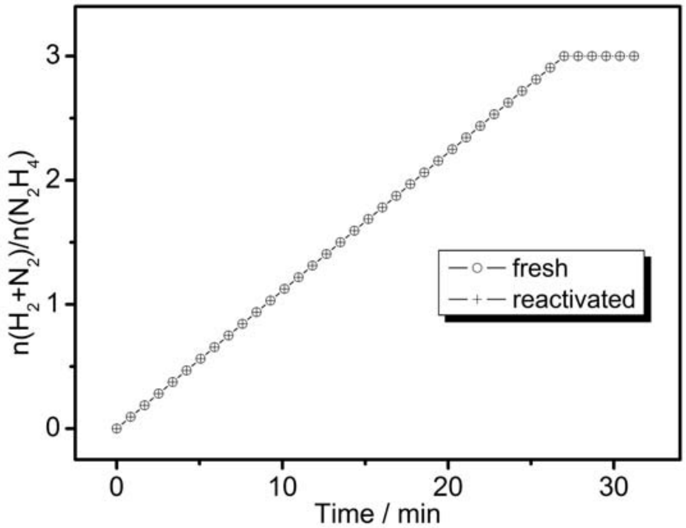

Fig.S19. Time profiles for decomposition of hydrous hydrazine in the presence (a) fresh and (b) reactivated Ni_3Fe/C

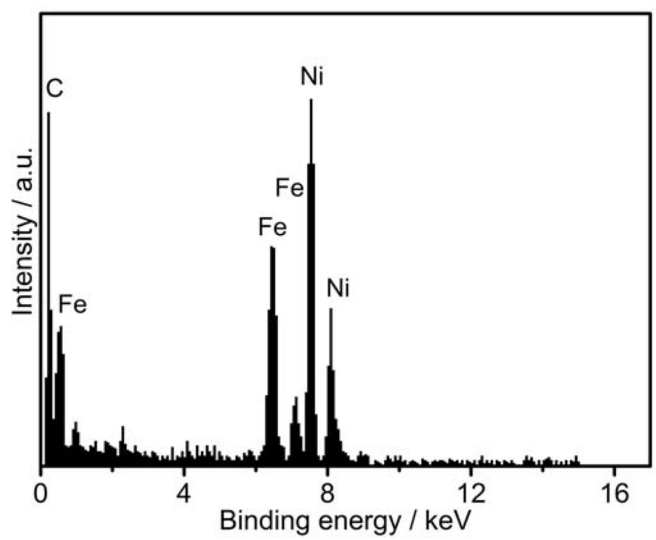

Fig.S20. EDS spectrum of the reactivated Ni_3Fe/C